Radiology

ORIGINAL RESEARCH • CARDIAC IMAGING

Anatomy-derived 3D Aortic Hemodynamics Using Fluid Physics–informed Deep Learning

Haben Berhane, MA[1,2] • *Anthony Maroun, MD*[1] • *David Dushfunian, MD*[1] • *Justin Baraboo, MS*[1] • *Gabriela Martinez, BS*[1] • *Tyler Jacobson, BS*[1,3] • *Ulas Bagci, PhD*[1,2] • *Bradley D. Allen, MD*[1] • *Michael Markl, PhD*[1,2]

Author affiliations, funding, and conflicts of interest are listed at the end of this article.

Radiology 2025; 315(2):e240714 • https://doi.org/10.1148/radiol.240714 • Content codes: CA AI

Background: Four-dimensional (4D) flow MRI provides assessment of thoracic aorta hemodynamic measures that are increasingly recognized as important biomarkers for risk assessment. However, long acquisition times and cumbersome data analysis limit widespread availability.

Purpose: To evaluate the feasibility and accuracy of a generative artificial intelligence (AI) approach (fluid physics–informed cycle generative adversarial network [FPI-CycleGAN]) in quantifying aorta hemodynamics directly from anatomic input as an alternative to 4D flow MRI.

Materials and Methods: Patients were retrospectively identified from a dataset of clinical cardiothoracic MRI examinations performed between November 2011 and July 2020. All patients underwent aortic 4D flow MRI, which served as a reference standard for training and testing of FPI-CycleGANs. A three-dimensional (3D) segmentation of the aortic geometry was used as the only input to predict systolic aortic hemodynamics, with separate networks for bicuspid aortic valve (BAV) (994 in the training set and 248 in the test set) and tricuspid aortic valve (TAV) (419 in the training set and 104 in the test set). Voxel-by-voxel and regional analyses were used to quantify and compare (AI vs the reference standard, 4D flow) systolic velocity vector fields, peak velocity, wall shear stress (WSS), and classification of aortic valve stenosis.

Results: In total, 1765 patients (median age, 53 years [IQR, 41–63 years]; 1242 patients had BAV and 523 had TAV) were included. Mean AI computation time was 0.15 second ± 0.11 (SD), and total training was 1500 and 3600 minutes for the TAV and BAV networks, respectively. The FPI-CycleGAN predicted systolic 3D velocity vector fields accurately, with low bias (<0.01 m/sec) and excellent limits of agreements (±0.06–0.08 m/sec). For peak velocities and WSS, there was strong agreement between FPI-CycleGAN and 4D flow (r^2 = 0.930–0.957 [P < .001], with relative differences of 6.2%–9.8%). AI accurately classified aortic valve stenosis severity in 85.8% of patients (302 of 352) (κ = 0.80 [95% CI: 0.71, 0.89]). The FPI-CycleGAN was robust to one- and two-voxel dilation and erosion (bias, −0.05 to 0.1 m/sec) and ±5° rotation (bias, −0.02 to 0.03 m/sec) of the input data. The application of the trained FPI-CycleGAN in an external test set with contrast-enhanced MR angiography (n = 60 patients) as AI input data demonstrated strong to excellent performance for peak velocities and WSS (r^2 = 0.944–0.965 [P < .001], with relative differences of 6.2%–9.2%).

Conclusion: Aorta 3D hemodynamics can be derived from anatomic input in less than 1 second using an FPI-CycleGAN and demonstrate strong agreement with in vivo 4D flow MRI systolic hemodynamics.

© RSNA, 2025

Supplemental material is available for this article.

Thoracic aortic diseases can lead to devastating complications, including aneurysm, dissection, and rupture. The most common birth defect of the heart, bicuspid aortic valve (BAV) (1), affects 1%–2% of the population and is associated with aortic complications in 40%–50% of patients. However, as outlined in the 2022 American Heart Association/American College of Cardiology guidelines (2), the current risk assessment paradigm based on simple aortic diameter thresholds has poor predictive value for aortic complications.

Four-dimensional (4D) flow MRI can be used to directly measure in vivo complex three-dimensional (3D) blood flow dynamics (hemodynamics) with volumetric coverage of the thoracic aorta (3,4). Many studies have demonstrated that 4D flow MRI provides insights into the relationships between aortic abnormalities and changes in 3D blood flow dynamics in the thoracic aorta (5–13). Growing evidence also supports that valve disease–mediated changes in ascending aorta hemodynamics, such as high velocity and elevated wall shear stress (WSS), drive aortic wall remodeling, growth, and adverse outcomes in patients with BAV (3,14–17).

Although 4D flow MRI is now considered the reference standard for the assessment and quantification of in vivo 3D blood flow dynamics in the aorta (18,19), several limitations impede the wider clinical translation and adoption of 4D flow MRI, including *(a)* lack of access to dedicated MRI systems and 4D flow MRI protocols, *(b)* limited test efficiency due to long 4D flow MRI examination times (5–12 minutes), and *(c)* burdensome and time-consuming postprocessing with dedicated software.

This study aimed to evaluate the feasibility and accuracy of a generative artificial intelligence (AI) approach (fluid physics–informed cycle generative adversarial network [FPI-CycleGAN]) in quantifying aorta hemodynamics directly from anatomic input as an alternative to systolic aorta hemodynamics derived from 4D flow MRI.

Materials and Methods

Study Sample

In this retrospective study, patients were identified from a single-center database of clinical cardiothoracic MRI examinations performed at a tertiary academic institution, including 4D flow MRI of the aorta, between November 2011 and July 2020. The study was compliant with the Health Insurance Portability and Accountability Act. The local institutional review board approved

This copy is for personal use only. To order copies, contact *reprints@rsna.org*

rory@cosmhq.com - December 19, 2025 - Read articles at www.DeepDyve.com

Abbreviations

AI = artificial intelligence, BAV = bicuspid aortic valve, CE MRA = contrast-enhanced MR angiography, FPI-CycleGAN = fluid physics–informed cycle generative adversarial network, 4D = four-dimensional, 3D = three-dimensional, TAV = tricuspid aortic valve, WSS = wall shear stress

Summary

A fluid physics–informed cycle generative adversarial network was successfully used to derive accurate three-dimensional aorta hemodynamics in less than 1 second using only aorta anatomic features as input data.

Key Results

- In this retrospective study of 1765 patients, a fluid physics–informed cycle generative adversarial network (FPI-CycleGAN) was developed as an alternative to systolic four-dimensional (4D) flow MRI–derived hemodynamics and provided aorta anatomy–derived systolic three-dimensional aortic hemodynamics in 0.15 second ± 0.11, with separate networks for patients with bicuspid aortic valve and tricuspid aortic valve.
- In internal test sets, the deep learning network strongly agreed with 4D flow MRI, particularly in predicted aortic peak velocities (r^2 = 0.930–0.957 [P < .001]; mean relative differences, 7.9%–9.8%) and was 85.8% accurate (302 of 352 patients) in classification of aortic valve stenosis severity.
- The FPI-CycleGAN was robust to one- and two-voxel dilation and erosion (bias, −0.05 to 0.1 m/sec) and ±5° rotation (bias, −0.02 to 0.03 m/sec) of the input data.

the study and waived the need for informed consent because of the use of deidentified data. Inclusion criteria were referral for clinical imaging assessment of aortic dimensions or aortic valve abnormalities. Aortic valve status (BAV or tricuspid aortic valve [TAV]) was derived from the medical records. Exclusion criteria were nonacquired 4D flow data, nonstandard 4D flow imaging volumes, nonstandard 4D flow protocol parameters, insufficient aorta 3D segmentation, and severe velocity aliasing. See Figure 1 and Appendix S1 for details.

4D Flow MRI Data Analysis

MRI data were acquired using either 1.5-T (n = 1512; Aera, Avanto, or Espree) or 3-T (n = 253; Skyra) MRI systems (all Siemens Healthineers) (Table S2). All patients were analyzed using a standardized 4D flow preprocessing workflow programmed in MATLAB (MathWorks), as described previously (20–25). A 3D phase contrast angiogram (26) was generated and used to create a 3D segmentation of the thoracic aorta (24). To visualize 3D blood flow velocity patterns, the peak systolic velocity vectors were visualized inside a 3D isosurface on the segmented aortic 3D geometry (Fig 2). Hemodynamic quantification included the calculation of a systolic velocity maximum intensity projection (Fig 3) and derivation of systolic WSS along the aorta wall (Fig 3) based on a previously reported method (27). Regional peak systolic velocities (top 5%) as well as maximum (top 5%) and median WSS were calculated in 3D regions of interest covering the ascending aorta, aortic arch, and descending aorta (28) (Appendix S1).

Deep Learning

Data flow and network architecture.—The data flow for developing a CycleGAN designed for the prediction of aorta hemodynamics is shown in Figure 2. The 3D segmentation of the aortic geometry was used as the input data, and the systolic 3D blood flow velocity vector field inside the aorta measured with 4D flow MRI served as ground truth data. The CycleGAN was composed of two generators and two discriminators (24,25). During network training, generator A derived hemodynamics, and discriminator A was used to distinguish between the AI-derived and 4D flow MRI ground truth data. The AI-derived 4D hemodynamics data were then fed to generator B to rederive the input (aortic 3D geometry), and discriminator B was used to distinguish between the original and AI-estimated aorta geometries.

Recognizing that aortic hemodynamics are driven not only by structure but also by the laws of fluid dynamics, fluid physics–informed constraints were incorporated into our generative AI models (29). These concepts included exploiting the well-known properties of blood as an incompressible fluid, which requires 3D velocity vector fields to meet divergence-free and flow momentum–balanced conditions. These conditions were mathematically expressed according to Navier-Stokes equations and integrated in the FPI-CycleGAN loss function. In addition, fluid physics constraints were augmented by minimizing the differences in velocity angle and magnitude between AI-derived and ground truth in vivo velocity vector fields. The final output was an AI-derived 3D velocity vector field (Vx, Vy, Vz) at peak systole, as shown in Figure 2C. See Appendix S1 for details. The code is available at *https://github.com/NUcvmri/CyclanGan-for-Aortic-Hemodynamics*.

Training and testing.—Separate FPI-CycleGANs were trained for patients with BAV or TAV. Eighty percent of patients with either BAV and TAV were randomly placed in the training set, and 20% were placed in the internal test set. For network training, 994 BAV and 419 TAV datasets were used. AI testing was performed on 248 BAV and 104 TAV datasets.

Classification of aortic valve stenosis.—Classification of aortic valve stenosis was based on ascending aorta peak systolic velocity and defined as none (≤2.5 m/sec), mild (>2.5 m/sec and ≤3.0 m/sec), moderate (>3.0 m/sec and <4.0 m/sec), or severe (≥4.0 m/sec).

Resilience to changes in input data.—The aortic geometry input to the FPI-CycleGAN was modified to assess the sensitivity and accuracy of the AI-produced output with imperfect inputs. The original aortic geometry was modified using one- and two-voxel erosion and dilation on the input 3D segmentation as well as a ±5° rotation along the z-axis. The FPI-CycleGAN was then re-executed for each internal test cohort patient with the modified input data to assess the robustness of the network for predicting the systolic 3D velocity vector field inside the aorta.

Contrast-enhanced MR angiography external test set.—To evaluate AI performance for different input data, the model was evaluated on a second external test set in 60 patients who belonged to the same study cohort and underwent additional contrast-enhanced MR angiography (CE MRA). The CE MRA data were used to create a 3D aorta segmentation, which served as input data to the FPI-CycleGAN. AI-derived peak systolic velocities and maximum WSS were calculated and compared

rory@cosmhq.com - December 19, 2025 - Read articles at www.DeepDyve.com

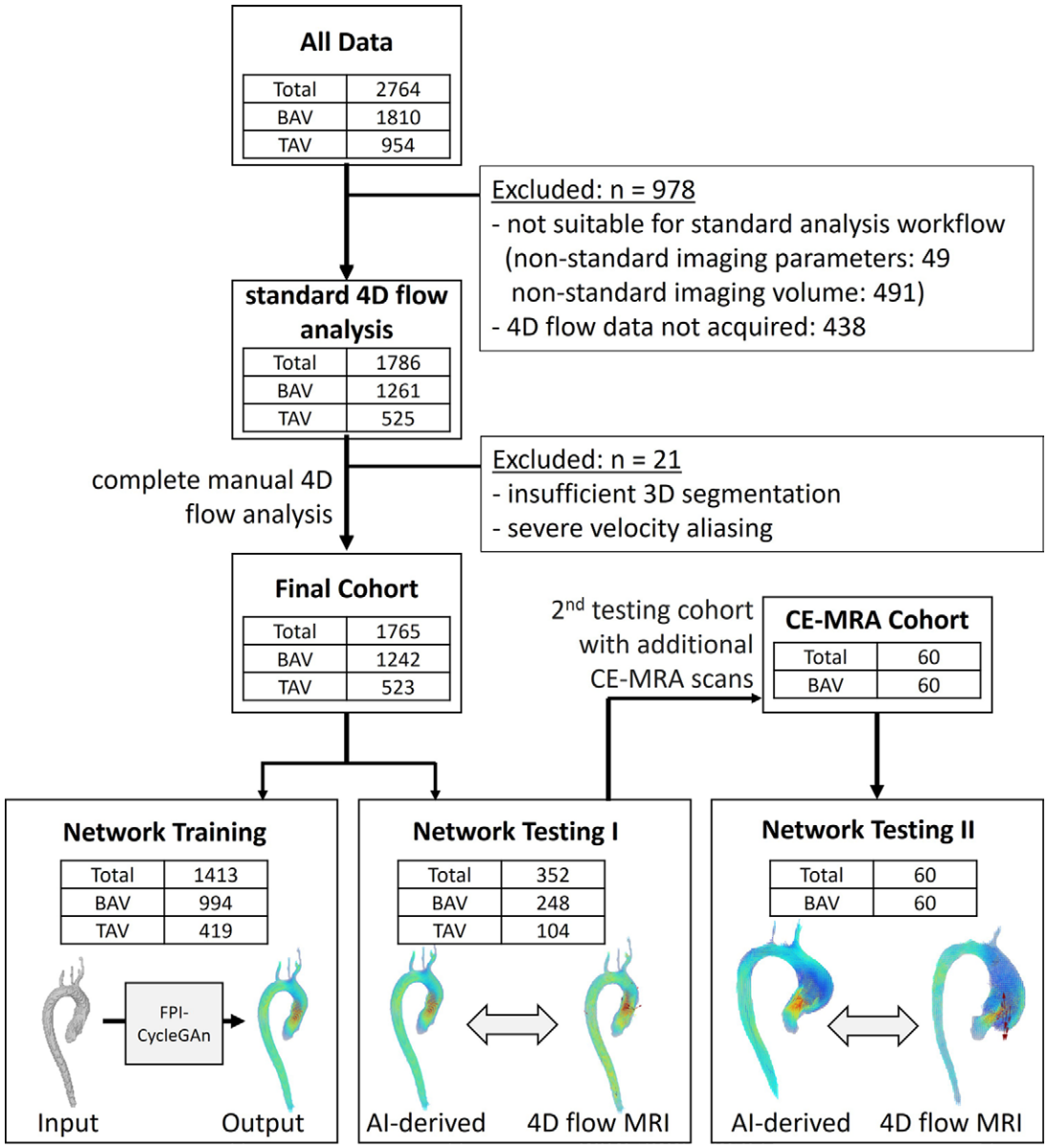

Figure 1: Study enrollment flowchart. A total of 2764 cardiothoracic MRI studies performed between November 2011 and July 2020 were queried for inclusion in this retrospective study. An 80%/20% split of the final study cohort was used for training and testing of the fluid physics–informed cycle generative adversarial network (FPI-CycleGAN). An additional external test set was used to assess the FPI-Cycle-GAN's performance with contrast-enhanced MR angiography (CE MRA) as network input data. AI = artificial intelligence, BAV = bicuspid aortic valve, 4D = four-dimensional, 3D = three-dimensional, TAV = tricuspid aortic valve.

with the patients' corresponding 4D flow MRI–derived velocities and WSS (ground truth data). None of the patients in the CE MRA cohort were included in the training set.

Statistical Analysis

Voxel-by-voxel comparisons were used to quantify the similarity of the AI-derived blood flow velocity magnitude and vector angles with ground truth 4D flow MRI results. Student *t* tests (or a nonparametric equivalent) were used to compare hemodynamic measures. Differences in hemodynamic parameters were compared using correlation and Bland-Altman analysis. To compare classification of aortic valve stenosis severity, agreement was assessed using the Cohen κ. $P < .05$ was considered to represent a statistically significant difference. Analyses were performed in MATLAB (R2020) by an author (H.B.).

Results

Patient Characteristics

A total of 2764 patients were identified in a single-center database of clinical cardiothoracic MRI examinations. Initially, 978 patients were excluded because of nonstandard 4D flow imaging volumes (n = 491), nonstandard 4D flow protocol parameters (n = 49), and nonacquired 4D flow data (n = 438). Additionally, 21 patients were excluded because of insufficient aorta 3D segmentation or severe velocity aliasing. A total of 1765 patients (age range, 17–91 years; median age, 53 years [IQR, 41–63 years]; 1269 male) were identified for final inclusion in the study cohort. Of the 1765 patients, 1242 had BAV (median age, 49 years [IQR, 38–60 years]; 902 male) and 523 had TAV (median age, 59 years [IQR, 50–68 years]; 367 male) (Table 1, Fig 1).

rory@cosmhq.com - December 19, 2025 - Read articles at www.DeepDyve.com

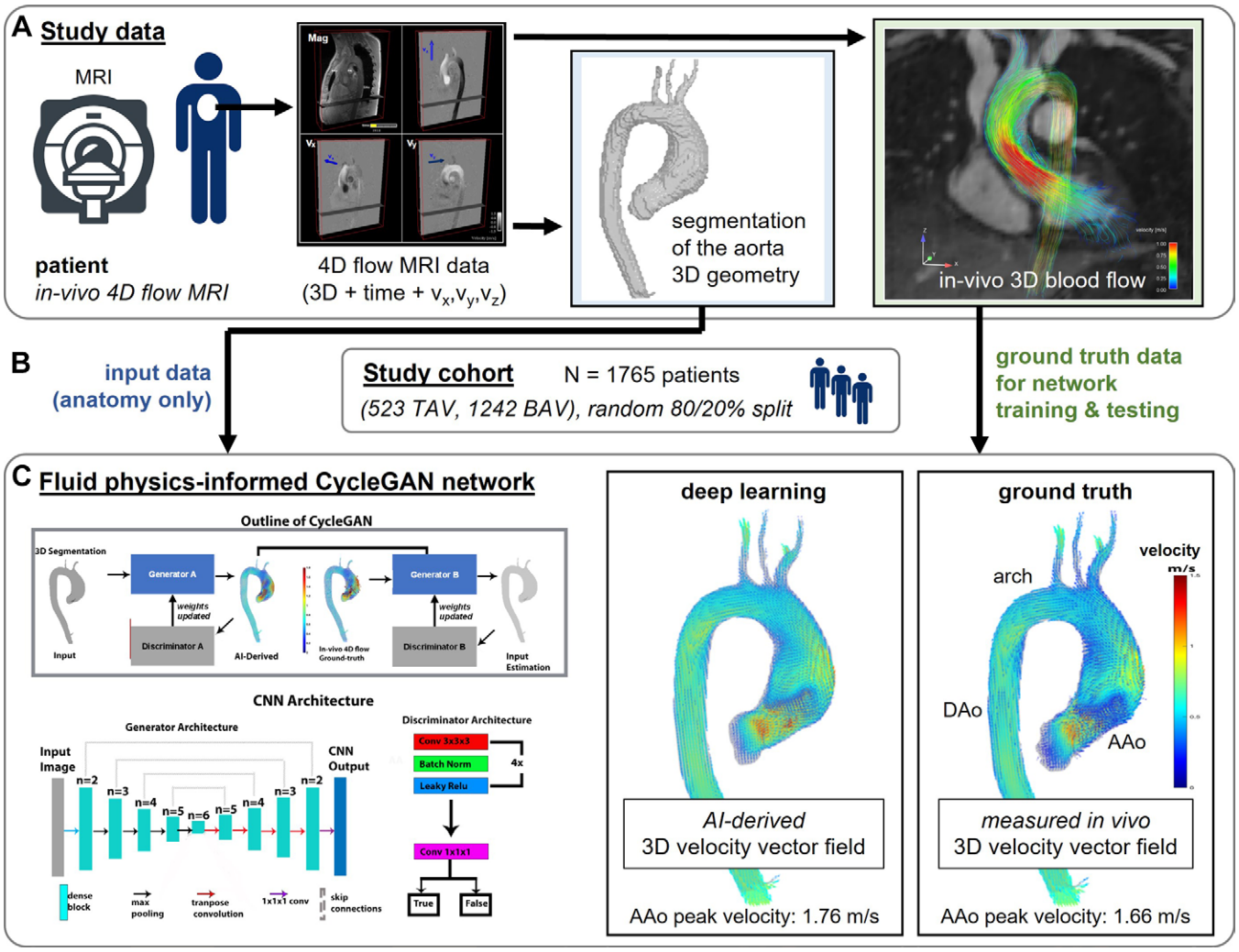

Figure 2: Illustration of the data flow and analysis pipeline for training and testing of a deep learning neural network (fluid physics–informed cycle generative adversarial network [FPI-CycleGAN]) to derive aortic hemodynamics (systolic three-dimensional [3D] blood flow velocity vector field) directly for anatomic imaging data (3D aorta geometry) as the only network input data. **(A)** The study data were obtained from patients undergoing surveillance MRI for aortic disease, including four-dimensional (4D) flow MRI of the thoracic aorta. The 4D flow data for each patient were used to derive a 3D segmentation of the thoracic aorta (FPI-CycleGAN input data) as well as for 3D aortic flow visualization and velocity quantification (FPI-CycleGAN ground truth data). **(B)** Training and testing of artificial intelligence (AI)–derived hemodynamics was based on a cohort total of 1765 patients. All patients underwent aortic 4D flow MRI, which served as the reference standard for the training and testing of a deep learning network to predict 4D aortic hemodynamics. **(C)** Outline of deep learning framework based on an FPI-CycleGAN neural network architecture. The FPI-CycleGAN is composed of two generators (blue boxes) and two discriminators (gray boxes). The network architecture of the generator and discriminator convolutional neural networks (CNNs) is shown below. The lower right panels present a side-by-side comparison of the aortic systolic 3D velocity vector fields, as generated by the neural network versus those measured using 4D flow MRI. The color coding represents velocity magnitude. AAo = ascending aorta, BAV = bicuspid aortic valve, conv = convolution, DAo = descending aorta, max = maximum, Relu = rectified linear units, TAV = tricuspid aortic valve.

Deep Learning Network Training

The total FPI-CycleGAN training times were 3600 minutes for the BAV network and 1500 minutes for the TAV network. Once network training was completed, inference time was a fraction of second, with a mean of 0.15 second ± 0.11 (SD) for both the BAV and TAV models.

BAV and TAV Aortic Peak Velocities and WSS

Figure 3 shows representative examples of AI-derived velocities and WSS compared with aortic 3D hemodynamics measured in vivo for patients with BAV and those with TAV. Side-by-side comparisons of peak systolic velocity and WSS derived using the FPI-CycleGAN network (Fig 3A) with those measured using 4D flow MRI (Fig 3B) show close agreement for velocity ranges and WSS patterns across the aorta.

This observation is corroborated by results across the entire internal test set (Fig 3C, 3D; Tables 2, 3; Table S3 for WSS results). Bland-Altman comparisons and correlation analyses demonstrated low nonsignificant bias (0.03–0.05 m/sec) and strong agreement (r^2 = 0.930–0.957; P < .001) between AI-derived and 4D flow–measured regional aortic peak velocities across the BAV and TAV datasets. The only differences in regional hemodynamic quantification was found for peak velocities in the ascending aorta for patients with TAV (AI-derived: 1.38 m/sec ± 0.18; in vivo: 1.33 m/sec ± 0.21; P = .006) and the descending aorta for patients with BAV (AI-derived: 0.85 m/sec ± 0.19; in vivo: 0.89 m/sec ± 0.21; P = .046) (Table 2). Nonetheless, mean relative differences between AI-derived and ground truth in vivo peak velocities ranged between 7.9% and 9.8% (ie, <10% and within the same range

rory@cosmhq.com - December 19, 2025 - Read articles at www.DeepDyve.com

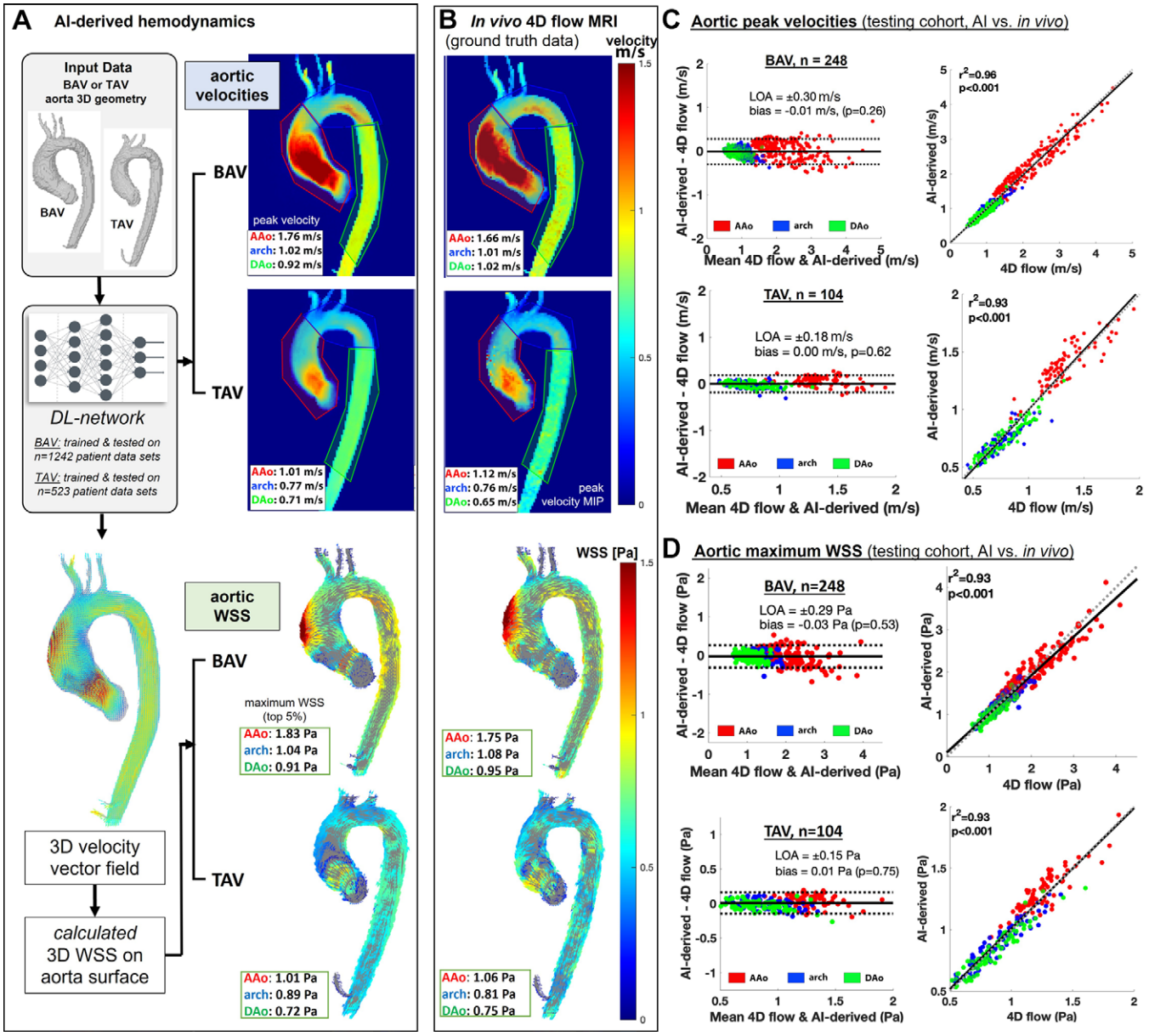

Figure 3: **(A)** Artificial intelligence (AI)–derived aortic peak systolic velocity maximum intensity projection (MIP) (top) and wall shear stress (WSS) (bottom) in example patients with bicuspid aortic valve (BAV) and normal tricuspid aortic valve (TAV) (color coding refers to velocity and WSS magnitude, respectively). The BAV or TAV thoracic aorta segmentation (three-dimensional [3D] geometry) served as input data for the deep learning (DL) network. **(B)** Aortic peak systolic velocity maximum intensity projections (top) and WSS (bottom) measured with in vivo four-dimensional (4D) flow MRI (ground truth data) show close agreement with AI-derived hemodynamics in **A** for velocity ranges and WSS patterns across the aorta. **(C, D)** Bland-Altman plots and correlation analysis comparing regional aortic peak velocities and maximum WSS across the BAV (left) and TAV (right) patient internal test sets show excellent agreement between AI-derived and in vivo 4D flow MRI–based velocity and WSS quantification. AAo = ascending aorta, DAo = descending aorta, LOA = limits of agreement.

as previously reported observer variability for in vivo 4D flow MRI analysis [20,30]).

No differences were observed for the median WSS across all aortic regions. For maximum WSS, only the ascending aorta in the TAV datasets showed a difference (AI-derived: 1.32 Pa ± 0.19; in vivo: 1.27 Pa ± 0.21; $P = .02$) (Table S3). The mean relative differences in both the median and maximum WSS were less than 10% (6.2%–8.5%).

BAV and TAV Systolic Aortic 3D Velocity Vector Field

Close correspondence between FPI-CycleGAN and 4D flow MRI results was also observed in comparison of individual velocity components (Vx, Vy, Vz) of the systolic 3D velocity vector fields on a voxel-by-voxel basis (Fig 4A). AI-derived aortic velocities agreed well with ground truth in vivo 4D flow MRI data, as denoted by minimal bias (<0.01 m/sec) and small limits of agreement (±0.06–0.08 m/sec) but significant differences ($P < .001$ for all). In addition, histogram analysis of voxel-by-voxel angular differences in velocity vectors between AI-derived and 4D flow MRI data (Fig 4B) revealed a small median vector angle difference of 9° across all 352 patients in the internal test set. Correlation analysis showed no associations between the absolute error of aorta peak velocities (AI-derived–4D flow) with velocity encoding sensitivity ($r = 0.12$; $P = .36$) or spatial resolution ($r = -0.06$; $P = .59$), indicating that these factors did not affect FPI-CycleGAN performance. No significant relationship was found for FPI-CycleGAN

rory@cosmhq.com - December 19, 2025 - Read articles at www.DeepDyve.com

Table 1: Characteristics of Study Cohort

	Network Training Set		Network Internal Test Set		CE MRA External Test Set
Characteristic	BAV	TAV	BAV	TAV	BAV
No. of patients	994	419	248	104	60
Age (y)*	52 (40–62)	60 (52–69)	50 (39–61)	61 (47–69)	49.5 (36–59)
BMI*†	26.3 (23.7–29.8)	27.1 (24.4–30.5)	25.8 (23.5–29.2)	27.5 (24.4–31.1)	25.5 (23.6–30.1)
Heart rate (beats/min)*	65 (59–73)	63 (57–71)	67 (60–75)	63 (57–70)	68 (60–77)
Sex					
M	722 (72.6)	289 (69.0)	180 (72.6)	78 (75.0)	38 (63.3)
F	272 (27.4)	130 (31.0)	68 (27.4)	26 (25.0)	22 (36.7)
Severity of aortic stenosis					
Severe	49 (4.93)	2 (0.48)	8 (3.22)	1 (0.96)	1 (1.67)
Moderate	84 (8.45)	8 (1.91)	23 (9.27)	3 (2.88)	9 (15.0)
Mild	374 (37.6)	80 (19.1)	84 (33.9)	17 (16.3)	17 (28.3)
None	487 (49.0)	329 (78.5)	133 (53.6)	83 (79.8)	33 (55.0)

Note.—Unless otherwise specified, data are numbers of patients, with percentages in parentheses. All percentages refer to the fraction of patients relative to the total number of patients in each column. BAV = bicuspid aortic valve, BMI = body mass index, CE MRA = contrast-enhanced MR angiography, TAV = tricuspid aortic valve.

* Data are medians, with IQRs in parentheses.

† BMI is calculated as weight in kilograms divided by height in meters squared.

Table 2: Peak Velocities for the Ascending Aorta, Aortic Arch, and Descending Aorta in Internal Test Set of 352 Patients

	Peak Velocities TAV			Peak Velocities BAV		
Variable	AAo	Arch	DAo	AAo	Arch	DAo
In vivo measured (m/sec)	1.33 ± 0.21	0.76 ± 0.15	0.79 ± 0.18	2.16 ± 0.73	1.04 ± 0.24	0.89 ± 0.21
AI-derived (m/sec)	1.38 ± 0.18	0.72 ± 0.12	0.76 ± 0.15	2.20 ± 0.66	1.00 ± 0.19	0.85 ± 0.19
P value	.006	.06	.25	.13	.06	.046
Difference (%)	8.2 ± 6.3 (7.0, 9.4)	8.3 ± 4.9 (7.4, 9.3)	7.1 ± 4.5 (6.2, 8.0)	9.8 ± 5.8 (9.1, 10.5)	8.8 ± 5.8 (8.1, 9.5)	7.9 ± 5.7 (7.2, 8.6)
AI-derived, erosion of input 3D aorta geometry (m/sec)						
One-voxel	1.38 ± 0.17*	0.72 ± 0.11	0.80 ± 0.15	2.24 ± 0.62*	0.98 ± 0.19	0.85 ± 0.17
Two-voxel	1.42 ± 0.18*	0.73 ± 0.12	0.78 ± 0.15	2.21 ± 0.61	0.97 ± 0.20*	0.85 ± 0.16
AI-derived, dilation of input 3D aorta geometry (m/sec)						
One-voxel	1.39 ± 0.18*	0.74 ± 0.12	0.76 ± 0.17	2.20 ± 0.64	1.03 ± 0.22	0.89 ± 0.19
Two-voxel	1.31 ± 0.18	0.71 ± 0.12	0.74 ± 0.14	2.13 ± 0.57	1.02 ± 0.21	0.88 ± 0.18
AI-derived, rotation of input 3D aorta geometry (m/sec)						
+5°	1.35 ± 0.24*	0.77 ± 0.18	0.80 ± 0.17	2.17 ± 0.67	1.03 ± 0.26	0.90 ± 0.21
−5°	1.31 ± 0.18*	0.79 ± 0.19	0.79 ± 0.17	2.18 ± 0.57	1.05 ± 0.21	0.87 ± 0.18

Note.—Unless otherwise specified, data are means ± SDs. Data in parentheses are 95% CIs. Relative differences between artificial intelligence (AI)–derived and ground truth in vivo peak velocities ranged between 7.9% and 9.8%; the only significant differences were found for peak velocities in the ascending aorta (AAo) among patients with tricuspid aortic valve (TAV) and the descending aorta (DAo) in patients with bicuspid aortic valve (BAV). 3D = three-dimensional.

* Indicates significant differences between peak velocities derived by AI and measured in vivo.

performance (absolute error) and the sex of the patients in the internal test set (P = .71).

Prediction of Aortic Valve Disease Severity

As shown in Figure 4C, the FPI-CycleGAN correctly identified aortic valve stenosis severity grade (none, mild, moderate, severe) in 85.8% of patients (302 of 352), with only minimal misclassification (no more than one grade difference in all misclassified patients). The κ score was 0.80 (95% CI: 0.71, 0.89), indicating substantial agreement with severity grading determined with 4D flow MRI data. Example cases for three patients with mild, moderate, and severe aortic valve stenosis (AI-derived 3D velocity vector fields vs 4D flow MRI ground truth data) are shown in Figure S1.

Resilience to Changes in Input Data

For one-voxel erosion and one-voxel dilation of the network input aorta geometry, AI performance was only mildly disturbed, with a small increase in bias (ascending aorta: 0.04–0.07 m/sec; arch: −0.05 to 0.0 m/sec; descending aorta: −0.04 to 0.01 m/sec) (Table 3). For two-voxel erosion and two-voxel dilation, greater discrepancies were observed, with an increased but

rory@cosmhq.com - December 19, 2025 - Read articles at www.DeepDyve.com

Table 3: Bland-Altman Results (Bias and Limits of Agreement for AI-derived vs In Vivo Measurements) for Systolic Peak Velocities of the Ascending Aorta, Aortic Arch, and Descending Aorta in Internal Test Set of 352 Patients

	Peak Velocities in Patients with TAV			Peak Velocities in Patients with BAV		
Variable	AAo	Arch	DAo	AAo	Arch	DAo
Original input 3D aorta geometry	0.05 ± 0.20	−0.04 ± 0.14	−0.03 ± 0.12	0.04 ± 0.41	−0.04 ± 0.21	−0.04 ± 0.15
Erosion of input 3D aorta geometry (m/sec)						
One-voxel	0.05 ± 0.22	−0.03 ± 0.15	0.01 ± 0.14	0.07 ± 0.46	−0.05 ± 0.21	−0.04 ± 0.18
Two-voxel	0.10 ± 0.24	−0.02 ± 0.17	−0.01 ± 0.17	0.05 ± 0.52	−0.05 ± 0.24	−0.04 ± 0.19
Dilation of input 3D aorta geometry (m/sec)						
One-voxel	0.07 ± 0.23	−0.01 ± 0.14	−0.02 ± 0.15	0.04 ± 0.47	0.0 ± 0.2	0.0 ± 0.16
Two-voxel	−0.01 ± 0.28	−0.03 ± 0.16	−0.04 ± 0.18	−0.03 ± 0.55	−0.01 ± 0.21	0.0 ± 0.19
Rotation of input 3D aorta geometry (m/sec)						
+5°	0.02 ± 0.22	0.0 ± 0.15	0.01 ± 0.11	−0.01 ± 0.43	−0.01 ± 0.20	0.0 ± 0.16
−5°	−0.02 ± 0.19	0.03 ± 0.17	0.0 ± 0.13	0.02 ± 0.42	0.01 ± 0.20	−0.01 ± 0.18

Note.—Data are mean bias ± limits of agreement. Bland-Altman comparisons demonstrate low nonsignificant bias and differences between artificial intelligence (AI)–derived and four-dimensional flow measured regional aortic peak velocities across the bicuspid aortic valve (BAV) and tricuspid aortic valve (TAV) internal test cohorts. Bland-Altman plots are provided in Figure S2. AAo = ascending aorta, DAo = descending aorta, 3D = three-dimensional,.

overall small bias compared with the ground truth 4D flow data (ascending aorta: −0.03 to 0.10 m/sec; arch: −0.05 to −0.01 m/sec; descending aorta: −0.04 to 0.0 m/sec) (Table 3). For ±5° rotations of the network input aorta geometry, only minor discrepancies compared with the original input data were observed (bias, ascending aorta: −0.02 to 0.02 m/sec; arch: −0.01 to 0.03 m/sec; descending aorta: −0.01 to 0.01 m/sec) (Tables 2, 3; Fig S2). Figures 5 and 6 show the patient cases with the best and worst network performance across the internal test set, as determined by the lowest (best) and highest (worst) mean difference at Bland-Altman analysis.

CE MRA External Test Set

Figure S3 shows examples of AI-derived systolic velocity and WSS derived from CE MRA input data. AI-derived peak velocities and maximum WSS showed strong agreement (r^2 = 0.944–0.965; P < .001) with 4D flow ground truth data. The only difference observed was for maximum WSS in the aortic arch (AI-derived: 1.13 Pa ± 0.22; 4D flow: 1.10 Pa ± 0.20; P = .03). The relative difference across all comparisons of peak velocity, median WSS, and maximum WSS was less than 10% (6.2%–9.2%) (Table S4).

Discussion

The evolving understanding of aorta hemodynamics and their complex interplay with aorta pathophysiology are crucial aspects of cardiovascular research and clinical care (31). This study shows that the integration of generative artificial intelligence techniques with fluid physics constraints has promise in deriving three-dimensional (3D) aortic hemodynamics from anatomic imaging data as the only network input. Main findings include the following: *(a)* a fluid physics–informed cycle generative adversarial network was successfully trained to provide aorta anatomy–derived systolic 3D aortic hemodynamics with less than 1 second in execution time and strong agreement compared with in vivo four-dimensional flow MRI ground truth data; *(b)* the network predicted aortic peak velocities and wall shear stress within limits of 10% and estimated the severity grade of aortic valve stenosis in close agreement with the clinical reference standard (r^2 = 0.930–0.957 [P < .001], with relative differences of 6.2%–9.8%); *(c)* the method was resilient to systematically applied changes to the network anatomic input data; and *(d)* application in an external test set with alternative input data (contrast-enhanced MR angiography) demonstrated strong performance (r^2 = 0.944–0.965 [P < .001], with relative differences of 6.2%–9.2%).

Several studies have demonstrated the utility of deep learning models for improved and automated 4D flow MRI data analysis workflows with increased efficiency (32–34) or to derive advanced hemodynamic measures (35,36). To our knowledge, our study shows the first use of machine learning to predict patient-specific hemodynamic information directly from anatomic input data without any additional boundary conditions. The application in a second CE MRA external test set supports the translatability of the technique to derive aortic hemodynamics from other anatomic input data. Previous studies have used deep learning to simulate fluid dynamics. Geneva and Zabaras (37) used a Bayesian deep neural network to improve the simulation of Reynolds-averaged turbulent flow. Others have highlighted the ability of neural networks to accelerate computational fluid dynamics simulation while being computationally less expensive (38,39). Zhang et al (40) reported on the development of physics-informed neural networks that used computational fluid dynamics to generate aortic flow velocity fields in two idealized model geometries. These results are promising for improving computational fluid dynamics–based approaches for simulating aortic hemodynamics. However, these studies were limited by the well-known challenge of defining precise anatomic and in-flow boundary conditions for numeric computational fluid dynamics calculations and the lack of real in vivo ground truth data of aortic 3D velocities in a large cohort of patients. In contrast, our machine learning technique was developed with 4D flow MRI data for network training, the current reference standard for the in vivo measurement of 3D aortic velocities (18,19), in a large patient cohort with thoracic aortic diseases or aortic valve abnormalities.

The choice for our AI model was motivated by previous success associated with the generative capabilities of cycle

rory@cosmhq.com - December 19, 2025 - Read articles at www.DeepDyve.com

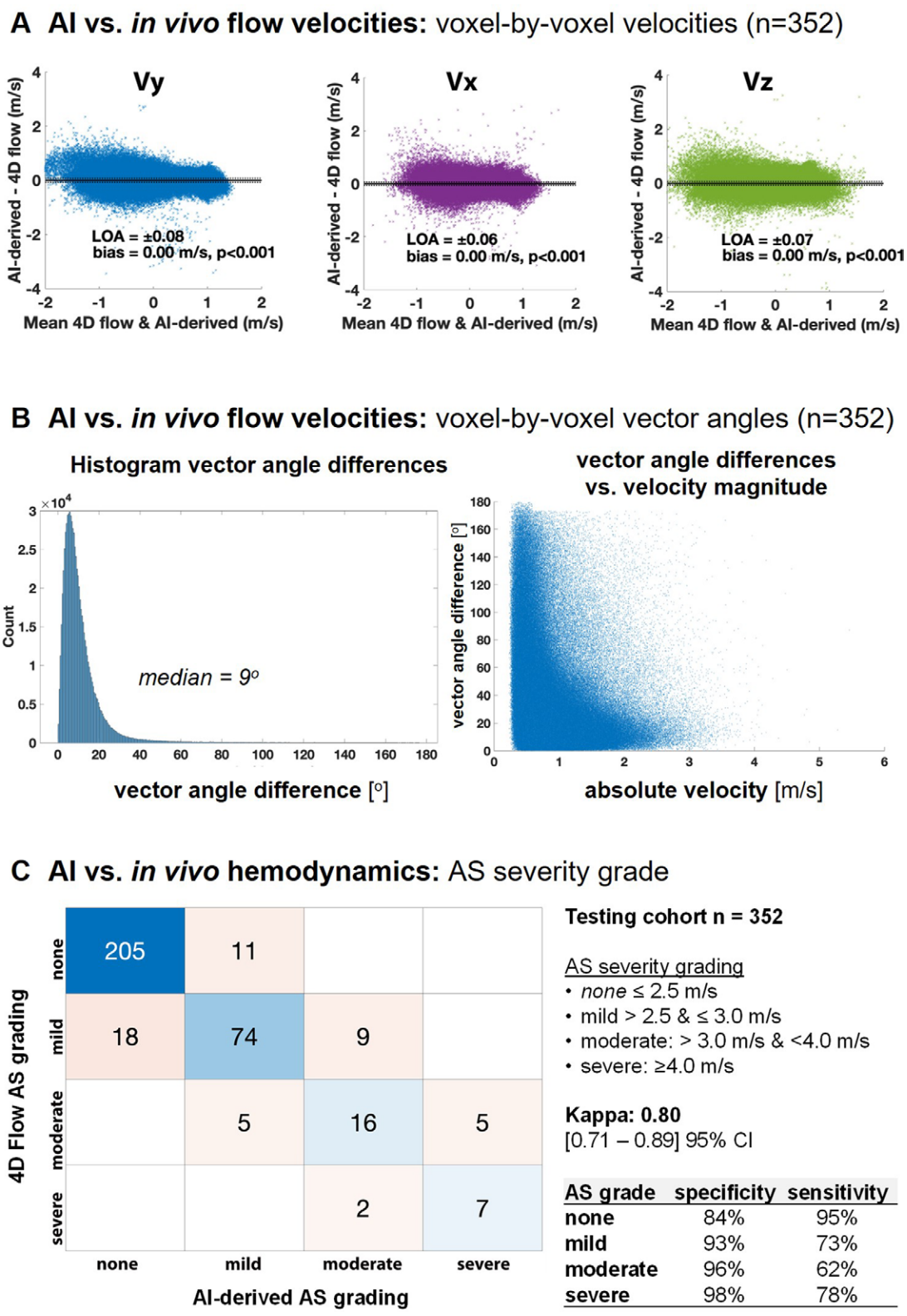

Figure 4: **(A)** Voxel-by-voxel Bland-Altman comparisons of artificial intelligence (AI)–derived versus measured in vivo aortic velocity vector components (Vx, Vy, Vz) for the entire test set (*n* = 352, patients with bicuspid and tricuspid aortic valve combined), indicating close agreement between fluid physics–informed cycle generative adversarial network and four-dimensional (4D) flow MRI–derived velocities. **(B)** Histogram (left) of voxel-by-voxel velocity angular difference between the AI-derived and 4D flow velocity vectors shows a vector angle difference (median, 9°) across all patients in the internal test set. Scatterplot (right) of the AI versus in vivo angular difference as a function of the absolute velocity across all voxels. The effect of velocity noise on deep learning performance (ie, increased angular differences for lower aortic velocities) can clearly be appreciated. **(C)** Severity grading of aortic valve stenosis (AS) determined with in vivo 4D flow MRI (ground truth) versus AI-derived hemodynamic quantification. On the basis of the ascending aorta peak velocities derived from the in vivo 4D flow MRI data, patient data were grouped as no stenosis (≤2.5 m/sec), mild stenosis (>2.5 and ≤3.0 m/sec), moderate stenosis (>3.0 and <4.0 m/sec), or severe stenosis (≥4.0 m/sec). A confusion matrix was generated based on the stenosis grading from the AI-derived and in vivo stenosis severity grades. A κ value of 0.80 indicates excellent agreement. LOA = limits of agreement.

rory@cosmhq.com - December 19, 2025 - Read articles at www.DeepDyve.com

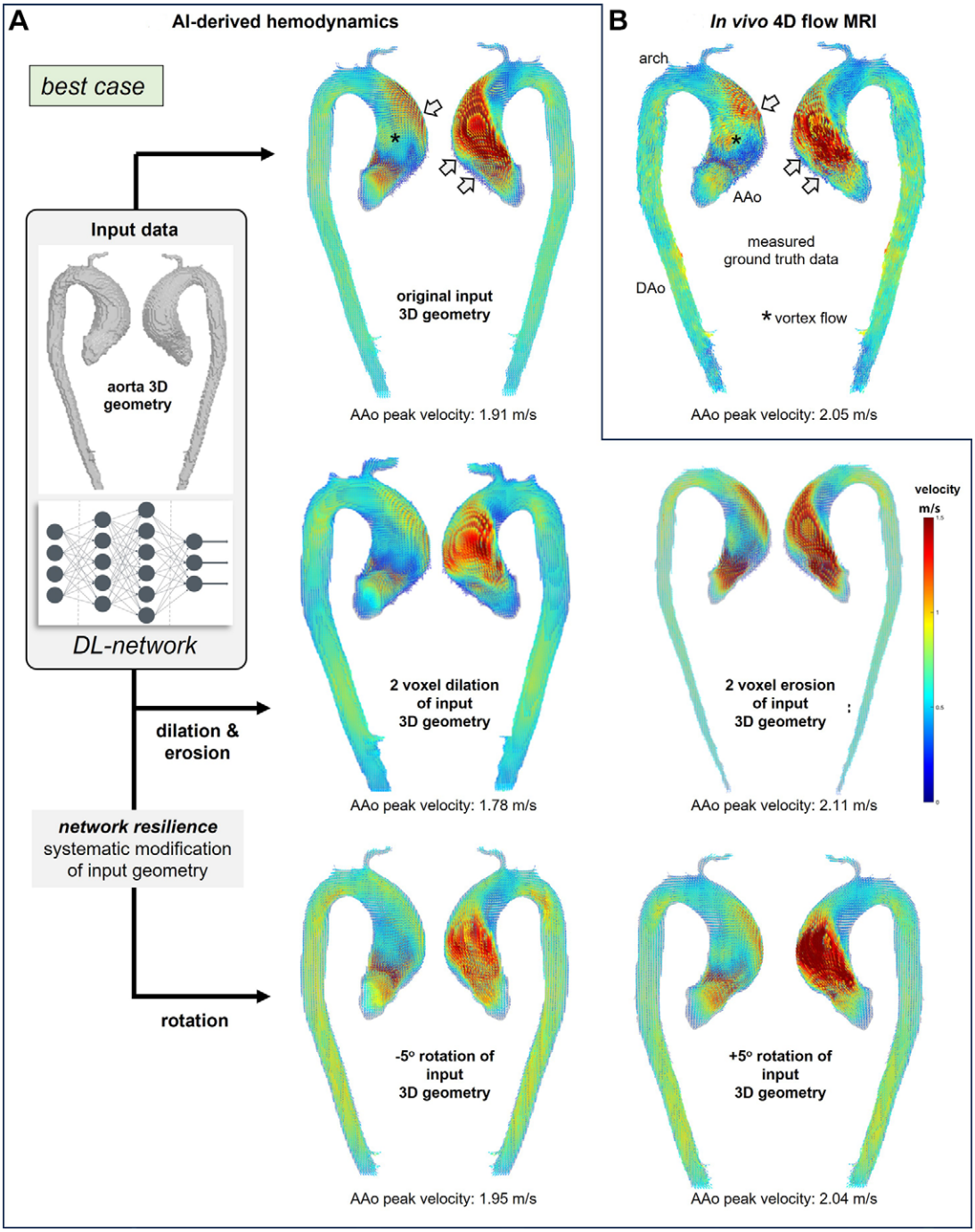

Figure 5: Aortic three-dimensional (3D) systolic blood flow velocity vector fields for the patient datasets with the best agreement between **(A)** artificial intelligence (AI)–derived hemodynamics and **(B)** in vivo four-dimensional (4D) flow MRI, as determined by the lowest mean difference at Bland-Altman analysis. **(A)** The thoracic aorta segmentation (3D geometry) served as input data for the deep learning (DL) network, which generated systolic 3D velocity vector fields. The color coding represents velocity magnitude. AI-derived velocity vector patterns (**A**, top left) closely resembled in vivo flow patterns measured with in vivo 4D flow MRI **(B)**, including a marked flow jet pattern along the left anterior wall (arrows) and vortex flow (marked by *) in the ascending aorta (AAo). The AI-derived 3D flow patterns remained consistent upon systematic testing of the effect of changes (two-voxel erosion, two-voxel dilation, and ±5° rotation) of the input 3D aorta geometry. DAo = descending aorta.

generative adversarial networks for applications in medical imaging (41–44). In addition, the primary clinical application of 4D flow MRI has been the evaluation of hemodynamic changes in the thoracic aorta. This focus provided access to the large dataset necessary for training and validating a trustable AI model capable of predicting aortic blood flow from anatomic input data. A large body of literature has shown differences in aortic hemodynamic patterns between patients with BAV and those with TAV (45). To address these distinctions, two separate networks were developed on the basis of aortic valve phenotype.

The fully trained networks could be executed in less than 1 second for each patient case on a standard desktop computer workstation. This points to the well-known advantage of deep learning solutions compared with alternative techniques, such as computational fluid dynamics, which are limited by long computation times to iteratively solve complex fluid dynamics

rory@cosmhq.com - December 19, 2025 - Read articles at www.DeepDyve.com

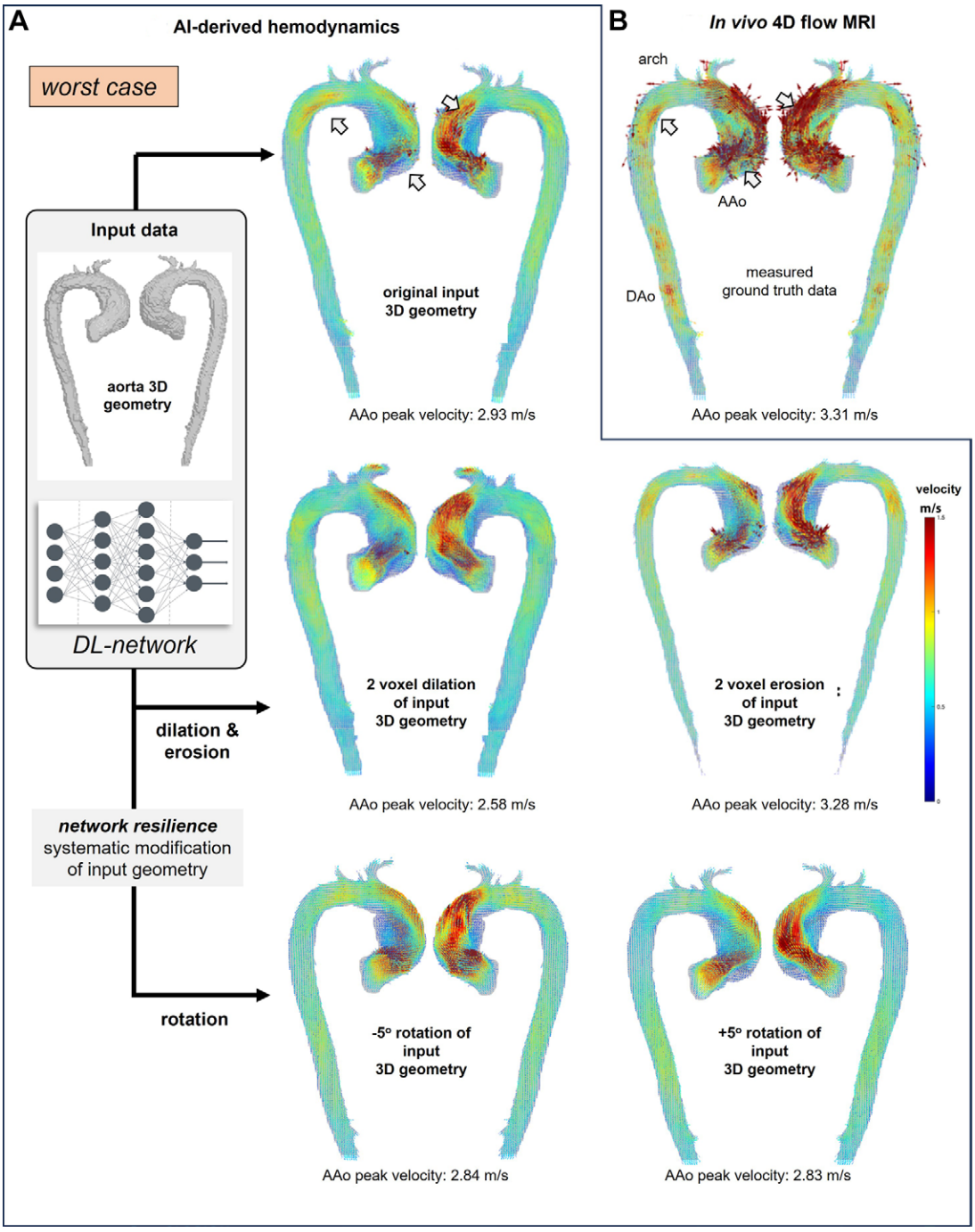

Figure 6: Aortic three-dimensional (3D) systolic blood flow velocity vector fields for the patient datasets with the worst agreement between **(A)** artificial intelligence (AI)–derived hemodynamics and **(B)** in vivo four-dimensional (4D) flow MRI, as determined by the largest mean difference at Bland-Altman analysis. **(A)** The thoracic aorta segmentation (3D geometry) served as input data for the deep learning (DL) network, which generated systolic 3D velocity vector fields. The color coding represents velocity magnitude. Despite discrepancies in ascending aorta (AAo) peak velocities, the deep learning network could reproduce systolic 3D velocity vector field estimations (**A**, top left) with similar high-velocity flow pattern (arrows) and velocity ranges compared with in vivo flow patterns measured with in vivo 4D flow MRI **(B)**. The AI-derived aortic flow patterns remained consistent upon systematic testing of the effect of changes (two-voxel erosion, two-voxel dilation, and ±5° rotation) of the input 3D aorta geometry. DAo = descending aorta.

equations. For reference, standard 4D flow MRI postprocessing can take 10–25 minutes (46); this difference suggests the potential for substantial time savings and workflow improvement to acquire hemodynamic information directly from anatomic images.

For patients with TAV, the only statistically significant difference in hemodynamic quantification was for peak velocities in the ascending aorta. We speculate that the reduced AI performance for TAV may be related to the smaller cohort for network training compared with the BAV network (419 with TAV vs 994 with BAV). However, the absolute difference between AI-derived and in vivo–measured peak velocities in the ascending aorta remained within acceptable ranges (<10% and similar to observer variability for in vivo 4D flow MRI analysis

rory@cosmhq.com - December 19, 2025 - Read articles at www.DeepDyve.com

[20,30]), underscoring the practical utility of the AI-derived results. This is supported by the small misclassification rate for aortic valve stenosis severity grading, where no more than one grade difference was observed. We also observed a shift to higher peak velocities for the ascending aorta when the input geometry was eroded but not dilated. This is likely the result of the erosion removing low-velocity voxels at the edge of the vessel, which may shift the velocity distribution and peak velocity toward higher velocities.

This study had a few limitations. First, the success and generalizability of AI models heavily depend on the quantity and quality of training data. Our current FPI-CycleGANs used single-center data and single-vendor 4D flow MRI sequence for network training and testing, which may limit application to patient data acquired at other intuitions and/or with different imaging systems and protocols. Furthermore, the approach to anatomy-derived aortic hemodynamics provided 3D flow velocity vector fields for only peak systole. However, the full characterization of flow changes requires dynamic information along the cardiac cycle to calculate functional parameters, such as stroke volume or regurgitant fraction. Our AI model focused on certain classes of cardiovascular disease (BAV or TAV aortopathy). If the input data (aortic 3D anatomy) lack critical information needed to differentiate various abnormalities, the model may face challenges in generalizing, even with extensive training data. In addition, an AI model based on limited or unrepresentative training data can carry the risk of overfitting (the model learns not only the underlying patterns in the training data but also random fluctuations specific to the dataset). Typically, this would result in a model that performs well on the training data but generalizes poorly to unseen data of the test set. Despite these limitations, our AI models demonstrated good to excellent performance, with low bias compared with the 4D flow ground truth data. Notably, this performance extended to alternative CE MRA input data, which was not included in the AI model's training set. Furthermore, although the current approach is tailored to BAV- and TAV-associated aortic valve diseases, it remains applicable to 2%–3% of the U.S. population affected by these conditions (1,2). Finally, the method is limited to 3D phase contrast angiography or CE MRA input data, and future work will expand this approach to other anatomic imaging, such as CT angiography. Preliminary results (Fig S4) indicate the feasibility of our approach to derive aortic hemodynamics based on more commonly available CT angiography input data. Future studies should explore FPI-CycleGAN performance for nonstandard acquisitions (eg, sagittal vs coronal vs axial input data) as well as other vascular territories.

The hemodynamic data generated from anatomic inputs using fluid physics–informed cycle generative adversarial networks showed strong agreement with four-dimensional flow MRI for peak systolic aortic hemodynamic assessment in less than 1 second. By providing easier access to aorta hemodynamics using only anatomic input, our development has the potential to expand the clinical role of hemodynamic analysis in patients with aortic disease. Future efforts should include further generalization of the artificial intelligence model to account for differences in site, scanning equipment vendor, and imaging protocols.

Deputy Editor: Rozemarijn Vliegenthart
Scientific Editor: Kate Vilas

Author affiliations:

[1] Department of Radiology, Feinberg School of Medicine, Northwestern University, 737 N Michigan Ave, Ste 1600, Chicago, IL 60611

[2] Department of Biomedical Engineering, McCormick School of Engineering, Northwestern University, Evanston, Ill

[3] Kellogg School of Management, Northwestern University, Evanston, Ill

Received March 13, 2024; revision requested April 23; final revision received March 3, 2025; accepted March 10.

Address correspondence to: M.M. (email: mmarkl@northwestern.edu).

Funding: Grant support from American Roentgen Ray Society Research Scholar Award, the Pat & Shirley Ryan Family Research Acceleration Fund, Dixon Foundation, and National Institutes of Health (R01-CA246704, R01-CA240639, U01-DK127384-02S1, U01-CA268808, T32-EB025766, and R42-HL174259).

Author contributions: Guarantors of integrity of entire study, **H.B., T.J., M.M.**; study concepts/study design or data acquisition or data analysis/interpretation, all authors; manuscript drafting or manuscript revision for important intellectual content, all authors; approval of final version of submitted manuscript, all authors; agrees to ensure any questions related to the work are appropriately resolved, all authors; literature research, **H.B., D.D., T.J., U.B., B.D.A., M.M.**; clinical studies, **B.D.A.**; experimental studies, **H.B., U.B., M.M.**; statistical analysis, **H.B., J.B., U.B., M.M.**; and manuscript editing, all authors

Disclosures of conflicts of interest: **H.B.** No relevant relationships. **A.M.** No relevant relationships. **D.D.** No relevant relationships. **J.B.** No relevant relationships. **G.M.** No relevant relationships. **T.J.** No relevant relationships. **U.B.** No relevant relationships. **B.D.A.** Grants to institution (Northwestern University) from Guerbet and the National Institutes of Health/National Heart, Lung, and Blood Institute (NIH/NHLBI) and grant to institution (Third Coast Dynamics) from NIH/NHLBI; consulting fees from Circle Cardiovascular Imaging; payment for lectures from Siemens, MRI Online, and Circle Cardiovascular Imaging; payment for expert testimony from Burns-White; payment for attending meetings and/or travel from Siemens; patents pending with Northwestern University; co-founder and president of Third Coast Dynamics; stock or stock options in Third Coast Dynamics. **M.M.** Grant support from Siemens and Circle Cardiovascular Imaging; co-founder of and shareholder in Third Coast Dynamics; deputy editor for *Radiology: Cardiothoracic Imaging*.

References

1. Siu SC, Silversides CK. Bicuspid aortic valve disease. J Am Coll Cardiol 2010;55(25):2789–2800.
2. Isselbacher EM, Preventza O, Hamilton Black J 3rd, et al; Peer Review Committee Members. 2022 ACC/AHA guideline for the diagnosis and management of aortic disease: a report of the American Heart Association/American College of Cardiology Joint Committee on Clinical Practice Guidelines. Circulation 2022;146(24):e334–e482.
3. Stankovic Z, Allen BD, Garcia J, Jarvis KB, Markl M. 4D flow imaging with MRI. Cardiovasc Diagn Ther 2014;4(2):173–192.
4. Azarine A, Garçon P, Stansal A, et al. Four-dimensional flow MRI: principles and cardiovascular applications. RadioGraphics 2019;39(3):632–648.
5. Rose MJ, Rigsby CK, Berhane H, et al. 4-D flow MRI aortic 3-D hemodynamics and wall shear stress remain stable over short-term follow-up in pediatric and young adult patients with bicuspid aortic valve. Pediatr Radiol 2019;49(1):57–67.
6. Bissell MM, Hess AT, Biasiolli L, et al. Aortic dilation in bicuspid aortic valve disease: flow pattern is a major contributor and differs with valve fusion type. Circ Cardiovasc Imaging 2013;6(4):499–507.
7. Mahadevia R, Barker AJ, Schnell S, et al. Bicuspid aortic cusp fusion morphology alters aortic three-dimensional outflow patterns, wall shear stress, and expression of aortopathy. Circulation 2014;129(6):673–682.
8. Reneman RS, Arts T, Hoeks APG. Wall shear stress—an important determinant of endothelial cell function and structure—in the arterial system in vivo. Discrepancies with theory. J Vasc Res 2006;43(3):251–269.
9. Silber HA, Bluemke DA, Ouyang P, Du YPP, Post WS, Lima JAC. The relationship between vascular wall shear stress and flow-mediated dilation: endothelial function assessed by phase-contrast magnetic resonance angiography. J Am Coll Cardiol 2001;38(7):1859–1865.
10. Malek AM, Alper SL, Izumo S. Hemodynamic shear stress and its role in atherosclerosis. JAMA 1999;282(21):2035–2042.

rory@cosmhq.com - December 19, 2025 - Read articles at www.DeepDyve.com

11. Hope MD, Hope TA, Crook SES, et al. 4D flow CMR in assessment of valve-related ascending aortic disease. JACC Cardiovasc Imaging 2011;4(7):781–787.
12. Hope MD, Hope TA, Meadows AK, et al. Bicuspid aortic valve: four-dimensional MR evaluation of ascending aortic systolic flow patterns. Radiology 2010;255(1):53–61.
13. den Reijer PM, Sallee D 3rd, van der Velden P, et al. Hemodynamic predictors of aortic dilatation in bicuspid aortic valve by velocity-encoded cardiovascular magnetic resonance. J Cardiovasc Magn Reson 2010;12(1):4.
14. Zilber ZA, Boddu A, Malaisrie SC, et al. Noninvasive morphologic and hemodynamic evaluation of type B aortic dissection: state of the art and future perspectives. Radiol Cardiothorac Imaging 2021;3(3):e200456.
15. Soulat G, Scott MB, Allen BD, et al. Association of regional wall shear stress and progressive ascending aorta dilation in bicuspid aortic valve. JACC Cardiovasc Imaging 2022;15(1):33–42.
16. Minderhoud SCS, Roos-Hesselink JW, Chelu RG, et al. Wall shear stress angle is associated with aortic growth in bicuspid aortic valve patients. Eur Heart J Cardiovasc Imaging 2022;23(12):1680–1689.
17. Guala A, Dux-Santoy L, Teixido-Tura G, et al. Wall shear stress predicts aortic dilation in patients with bicuspid aortic valve. JACC Cardiovasc Imaging 2022;15(1):46–56.
18. Bissell MM, Raimondi F, Ait Ali L, et al. 4D flow cardiovascular magnetic resonance consensus statement: 2023 update. J Cardiovasc Magn Reson 2023;25(1):40.
19. Dyverfeldt P, Bissell M, Barker AJ, et al. 4D flow cardiovascular magnetic resonance consensus statement. J Cardiovasc Magn Reson 2015;17(1):72.
20. Schnell S, Entezari P, Mahadewia RJ, et al. Improved semiautomated 4D flow MRI analysis in the aorta in patients with congenital aortic valve anomalies versus tricuspid aortic valves. J Comput Assist Tomogr 2016;40(1):102–108.
21. Bernstein MA, Zhou XJ, Polzin JA, et al. Concomitant gradient terms in phase contrast MR: analysis and correction. Magn Reson Med 1998;39(2):300–308.
22. Walker PG, Cranney GB, Scheidegger MB, Waseleski G, Pohost GM, Yoganathan AP. Semiautomated method for noise reduction and background phase error correction in MR phase velocity data. J Magn Reson Imaging 1993;3(3):521–530.
23. Bock JKB, Hennig J, Markl M. Optimized pre-processing of time-resolved 2D and 3D Phase Contrast MRI data. 15th Annual Meeting of ISMRM Berlin, German. 2007; Abstract 3138. https://cds.ismrm.org/protected/07MProceedings/PDFfiles/03138.pdf.
24. Berhane H, Scott M, Elbaz M, et al. Fully automated 3D aortic segmentation of 4D flow MRI for hemodynamic analysis using deep learning. Magn Reson Med 2020;84(4):2204–2218.
25. Berhane H, Scott MB, Barker AJ, et al. Deep learning-based velocity antialiasing of 4D-flow MRI. Magn Reson Med 2022;88(1):449–463.
26. Markl M, Harloff A, Bley TA, et al. Time-resolved 3D MR velocity mapping at 3T: improved navigator-gated assessment of vascular anatomy and blood flow. J Magn Reson Imaging 2007;25(4):824–831.
27. van Ooij P, Potters WV, Collins J, et al. Characterization of abnormal wall shear stress using 4D flow MRI in human bicuspid aortopathy. Ann Biomed Eng 2015;43(6):1385–1397.
28. Rose MJ, Jarvis K, Chowdhary V, et al. Efficient method for volumetric assessment of peak blood flow velocity using 4D flow MRI. J Magn Reson Imaging 2016;44(6):1673–1682.
29. Halder S, Acharya S, Kou W, Kahrilas PJ, Pandolfino JE, Patankar NA. Mechanics informed fluoroscopy of esophageal transport. Biomech Model Mechanobiol 2021;20(3):925–940.
30. van Ooij P, Powell AL, Potters WV, Carr JC, Markl M, Barker AJ. Reproducibility and interobserver variability of systolic blood flow velocity and 3D wall shear stress derived from 4D flow MRI in the healthy aorta. J Magn Reson Imaging 2016;43(1):236–248.
31. Rodríguez-Palomares JF, Dux-Santoy L, Guala A, Galian-Gay L, Evangelista A. Mechanisms of aortic dilation in patients with bicuspid aortic valve: *JACC* state-of-the-art review. J Am Coll Cardiol 2023;82(5):448–464.
32. Bustamante M, Viola F, Engvall J, Carlhäll CJ, Ebbers T. Automatic time-resolved cardiovascular segmentation of 4D flow MRI using deep learning. J Magn Reson Imaging 2023;57(1):191–203.
33. Corrado PA, Seiter DP, Wieben O. Automatic measurement plane placement for 4D flow MRI of the great vessels using deep learning. Int J CARS 2022;17(1):199–210.
34. Garrido-Oliver J, Aviles J, Córdova MM, et al. Machine learning for the automatic assessment of aortic rotational flow and wall shear stress from 4D flow cardiac magnetic resonance imaging. Eur Radiol 2022;32(10):7117–7127.
35. Ferdian E, Dubowitz DJ, Mauger CA, Wang A, Young AA. WSSNet: aortic wall shear stress estimation using deep learning on 4D flow MRI. Front Cardiovasc Med 2022;8:769927.
36. Nath R, Kazemi A, Callahan S, Stoddard MF, Amini AA. 4Dflow-VP-Net: a deep convolutional neural network for noninvasive estimation of relative pressures in stenotic flows from 4D flow MRI. Magn Reson Med 2023;90(5):2175–2189.
37. Geneva N, Zabaras N. Quantifying model form uncertainty in Reynolds-averaged turbulence models with bayesian deep neural networks. J Comput Phys 2019;383:125–147.
38. Calzolari G, Liu W. Deep learning to replace, improve, or aid CFD analysis in built environment applications: a review. Build Environ 2021;206:108315
39. Vinuesa R, Brunton SL. Enhancing computational fluid dynamics with machine learning. Nat Comput Sci 2022;2(6):358–366.
40. Zhang X, Mao B, Che Y, et al. Physics-informed neural networks (PINNs) for 4D hemodynamics prediction: an investigation of optimal framework based on vascular morphology. Comput Biol Med 2023;164:107287.
41. Zhu JY, Park T, Isola P, Efros AA. Unpaired image-to-image translation using cycle-consistent adversarial networks. 2017.
42. Gu X, Knutsson H, Nilsson M, Eklund A. Generating diffusion MRI scalar maps from T1 weighted images using generative adversarial networks. In: Felsberg M, Forssén PE, Sintorn IM, Unger J, eds. Image Analysis. SCIA 2019. Lecture Notes in Computer Science, vol 11482. Springer, Cham.
43. Liu Y, Chen A, Shi H, et al. CT synthesis from MRI using multi-cycle GAN for head-and-neck radiation therapy. Comput Med Imaging Graph 2021;91:101953.
44. Zhang H, Li H, Dillman JR, Parikh NA, He L. Multi-contrast MRI image synthesis using switchable cycle-consistent generative adversarial networks. Diagnostics (Basel) 2022;12(4):816.
45. van Ooij P, Markl M, Collins JD, et al. Aortic valve stenosis alters expression of regional aortic wall shear stress: new insights from a 4-dimensional flow magnetic resonance imaging study of 571 subjects. J Am Heart Assoc 2017;6(9):e005959.
46. Burkhardt BEU, Kellenberger CJ, Callaghan FM, Valsangiacomo Buechel ER, Geiger J. Flow evaluation software for four-dimensional flow MRI: a reliability and validation study. Radiol Med (Torino) 2023;128(10):1225–1235.

rory@cosmhq.com - December 19, 2025 - Read articles at www.DeepDyve.com